ELSEVIER

European Journal of Mechanics B/Fluids 21 (2002) 171–183

EUROPEAN JOURNAL OF MECHANICS B/FLUIDS

A model of flapping motion in a plane jet

Oliver V. Atassi *, Richard M. Lueptow

Department of Mechanical Engineering, Northwestern University, Evanston, IL 60208, USA

Received 3 July 2000; received in revised form 5 July 2001; accepted 8 November 2001

Abstract

Flow visualization near the exit of a plane jet shows a small-amplitude disturbance whose wavelength is large relative to the jet shear layer thickness. Further downstream, in the transition region, concentrated regions of vorticity are observed which drive the flapping motion of the jet. These observations motivate an inviscid, two-dimensional model for the transitional region of the jet. Linear stability analysis of a piecewise-uniform shear layer model indicates that small-amplitude, long wavelength disturbances are unstable. Long wave theory shows that regions of high circulation convect downstream faster than regions of low circulation resulting in nonlinear steepening and that the rate of the steepening is directly proportional to the strength of the local shear. The long wave theory also shows that finite-amplitude sinuous disturbances at the jet centerline will grow linearly as they convect downstream. The results predict the steepening and growth of the jet centerline observed in the flow visualization.

Keywords: Plane jet; Stability; Long wave theory

1. Introduction

Experiments [1–9] indicate that a planar, turbulent jet with high aspect ratio has an organized two-dimensional structure that plays an important role in the flapping motion and transfer of momentum between the irrotational (outer) flow and the shear layer. The flapping motion was originally suggested based on the quasi-periodic negative cross-correlation between the fluctuating longitudinal velocities on either side of the jet centerline [2]. At high Reynolds numbers, the 'flapping' frequency was shown to be Reynolds number independent when non-dimensionalized by the local mean velocity and the local jet half-width [5] suggesting an inviscid mechanism for the flapping motion. In addition, these experiments indicate the existence of large-scale, quasi two-dimensional, counter-rotating vortices which propagate periodically downstream like a Karman vortex street and which occur in the transition region where the two mixing layers merge to form a single mixing layer. Antonia et al. [8] performed experiments to determine the topology of these structures and measure their contribution to the momentum and heat transport relative to the transport due to the random motions. In a reference frame moving with the centers of the stuctures, they observed that the jet consists of adjacent vortical structures whose vorticity is antisymmetric relative to the jet centerline.

The aformentioned papers describe the spatial structure of the plane jet and show that concentrated regions of vorticity play a major role in the flapping motion. In an attempt to study the nonlinear process by which concentrated regions of vorticity develop, multi-layer models with simple vorticity distributions have been studied. Rayleigh [10] first considered small-amplitude disturbances to a piecewise-linear shear layer where the magnitude of the vorticity above and below the centerline of the jet was equal. He found that small-amplitude disturbances are unstable for long wavelengths. Stern and Vorapayev [11], motivated by the formation of vorticity fronts in geophysical flows, extended the uniform vorticity model to finite-amplitude disturbances and showed that steepening fronts of vorticity formed from initially long wavelength disturbances. They considered

* Corresponding author. Current address: Pratt & Whitney, E. Hartford, CT, USA.
E-mail address: atassio@pweh.com (O.V. Atassi).

0997-7546/02/$ – see front matter
PII: S0997-7546(01)01176-1

only varicose disturbances which, due to their symmetry, are analogous in an inviscid flow to a wall-bounded shear layer. Similarly Jimenez and Orlandi [12], motivated by the formation of streamwise vortices in turbulent boundary layers, showed that wall-bounded shear layers can develop into concentrated regions of vorticity.

In the present work, we extend the work of Stern and Vorapayev [11] and Jimenez and Orlandi [12] to consider nonsymmetric disturbances to a shear layer with arbitrary vorticity and show that concentrated fronts of vorticity may develop and steepen. In Section 2, we present flow visualization of the near-exit and transition regions of the jet. Near the exit, small-amplitude sinuous disturbances are observed which further downstream evolve into large-amplitude steeply-sloping disturbances apparently driven by counterrotating concentrated regions of vorticity on opposite sides of the jet centerline. These results motivate an inviscid model of a shear layer where the mean vorticity in the upper layer is positive and the mean vorticity in the lower layer is negative. In Section 3, we present linear stability analysis for the uniform vorticity case and find that small-amplitude nonsymmetric disturbances are unstable to long wavelengths. As a result, we examine the evolution of finite-amplitude long wavelength disturbances for both an arbitrary continuous distribution of vorticity and for a discontinuous but uniform distribution of vorticity.

2. Flow visualization of a planar jet

A two-dimensional jet was generated using a planar vertical slot $D = 0.5$ cm wide and 17.2 cm high in a 42.6 cm wide by 120 cm long tank filled with water to a depth of 30.5 cm, as shown in Fig. 1. A pump supplied water to a stack of tubes trapped between the upstream end of slightly converging acrylic plates with a streamwise length of $55D$ that form a slot nozzle. The uniformity of the jet exit velocity along the length of the slot was measured with a pitot tube and was within 2% except at the ends of the slot. Vertical face plates at the nozzle exit plane ensured that fluid from behind the nozzle exit was not entrained in the jet. The jet exit was $160D$ from the downstream end of the tank. A laser sheet in a horizontal plane at the midpoint of the slot was used to illuminate tracer particles (14×10^{-6} m diameter silver-coated hollow glass spheres) in the jet fluid. The tracer particles remain in suspension for a time that is orders of magnitude longer than the experiment. No particles were initially in the tank fluid. The flow was recorded using a CCD camera.

A computer-enhanced image of tracer particles in the transition region of a planar jet at a Reynolds number of $Re = 173$ (based on the slot-width and average jet exit velocity) is shown in Fig. 2 over a streamwise domain of $4.8D < x < 16.6D$ downstream of the nozzle exit. The tracer particles mark the jet fluid. The jet consists of an undulating shear layer with its main component of velocity in the streamwise direction. The unmarked outer region consists of quiescent irrotational flow that is eventually entrained by the jet. The few particles lying in the unmarked region are stray particles from a previous experiment. The sinuous character, or flapping motion, of the jet is evident in the upstream portion of the jet. Consecutive images of the flow field indicate that the waviness of the shear layer propagates downstream with the mean flow. The perturbations are non-symmetric, or sinuous, with respect to the jet centerline, consistent with the result of our stability analysis, presented in the next section, which indicates that non-symmetric modes are unstable. The lengthscale of the sinuous motion is about $3D$, on the order of the streamwise scale of the experiment, whereas the inner shear layer is much smaller. This result motivates our nonlinear long wave theory, presented later in this paper.

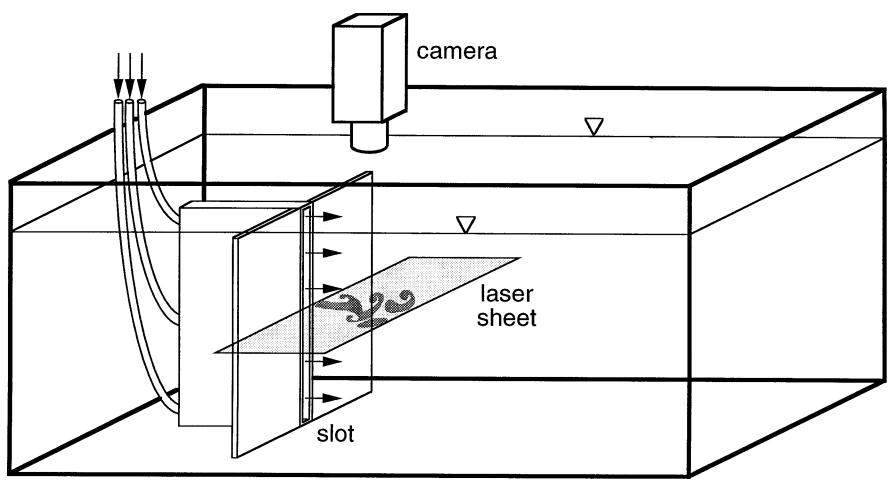

Fig. 1. A schematic of the experimental setup (not to scale). Only 3 of the many tubes entering the slot are shown.

Fig. 2. A computer-enhanced image of tracer particles in a plane perpendicular to the jet slot for $4.8D \times 6.6D$ downstream from the jet exit at $Re = 173$.

The frequency of the flapping motion is about 3 Hz, corresponding to a dimensionless frequency of 0.2 based on the mean velocity at the jet exit and the slot half-width. The Reynolds number of 173 also suggests that the timescale of the inertial flapping motion is fast compared to the timescale of viscous diffusion and, as a result, the flapping motion is driven by an inviscid mechanism. Thus, the use of an inviscid model of the flow in the following sections is reasonable. Also evident in Fig. 2 is an apparent steepening of the sinuous disturbances and the formation of downstream rotating coherent structures antisymmetric with respect to the jet centerline. Like the waviness of the central shear layer, the rotating coherent structures translate downstream.

3. Model formulation and results

We model the jet as two-dimensional, incompressible and inviscid. The flow is decomposed into four regions where the vortical regions II and III in Fig. 3 are bounded above and below by irrotational regions I and IV. The interface $y = H_+(x,t)$ separates the irrotational flow from the layer of positive vorticity, the interface $y = H_0(x,t)$ separates the positive and negative vorticity regions, and the interface $y = H_-(x,t)$ separates the negative vorticity layer from the irrotational flow below it. The three interfaces located at $y = H_+(x,t)$, $y = H_0(x,t)$, and $y = H_-(x,t)$ approach the unperturbed mean values $y = H_+^{(\infty)}, 0$, and $H_-^{(\infty)}$ as $|x| \to \infty$. We non-dimensionalize all lengths with respect to $H_+^{(\infty)}$ and time with respect to the mean vorticity as $|x| \to \infty$ in region II, $1/\omega_+^{(\infty)}$.

We introduce a stream function, $\psi(x,y,t)$, such that the streamwise and transverse velocities

$$\left(u^j, v^j\right) = \left(\frac{\partial \psi^j}{\partial y}, -\frac{\partial \psi^j}{\partial x}\right), \tag{1}$$

where $j = \mathrm{I}, \mathrm{II}, \mathrm{III}, \mathrm{IV}$ is used to denote the regions I–IV. Note that although we use the superscripts to denote the stream function in each region, the stream function is continous across all four regions. The stream function satisfies Laplace's equation in regions I and IV and Poisson's equation in regions II and III. This is expressed as

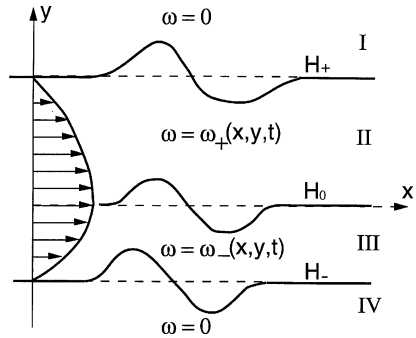

Fig. 3. Piecewise linear model of an asymmetric planar jet.

$$\begin{aligned}
&\nabla^2\psi^{\mathrm{I}}(x,y,t) = 0, \quad y > H_+(x,t),\\
&\nabla^2\psi^{\mathrm{II}}(x,y,t) = -\omega_+(x,y,t), \quad H_0(x,t) < y < H_+(x,t),\\
&\nabla^2\psi^{\mathrm{III}}(x,y,t) = -\omega_-(x,y,t), \quad H_-(x,t) < y < H_0(x,t),\\
&\nabla^2\psi^{\mathrm{IV}}(x,y,t) = 0, \quad y < H_-(x,t).
\end{aligned} \tag{2}$$

In the limit of uniform vorticity equal to $\omega_+^{(\infty)}$ in region II and equal to $\omega_-^{(\infty)}$ in region III, $\omega_+ \to 1$ and $\omega_- \to \beta$ where $\beta = \omega_-^{(\infty)}/\omega_+^{(\infty)} = H_+^{(\infty)}/H_-^{(\infty)}$ is a measure of the asymmetry of the jet and implies that the total circulation of the unperturbed jet equals zero. The model reduces to that considered by Rayleigh [10] in the limit as β goes to -1.

The vorticity in regions II and III evolves according to the vorticity transport equation

$$\frac{D}{Dt}\omega = 0, \tag{3}$$

where $D/Dt \equiv \partial/\partial t + \mathbf{u}\cdot\boldsymbol{\nabla}$. We impose the kinematic condition that points initially on an interface will remain on the interface yielding

$$v = \frac{\partial H_{(+,0,-)}}{\partial t} + u\frac{\partial H_{(+,0,-)}}{\partial x}, \quad y = H_{(+,0,-)}. \tag{4}$$

Across each interface the transverse velocity and the pressure are continuous:

$$\left(v^{\mathrm{I,II,III}}, p^{\mathrm{I,II,III}}\right) = \left(v^{\mathrm{II,III,IV}}, p^{\mathrm{II,III,IV}}\right), \quad y = H_{(+,0,-)}. \tag{5}$$

In Subsection 3.1, we briefly examine the linear stability of the jet in the uniform vorticity limit. The results of this subsection motivate the nonlinear long wave analysis in Subsection 3.2 where a continuously varying distribution of vorticity is assumed. In Subsection 3.3, we consider specific cases of the general long wave theory to obtain solutions for the motion of the interfaces and to examine the effect of vorticity distribution and the type of disturbance, sinuous or varicose, on the evolution of the jet shear layers.

3.1. Stability of the jet to small disturbances in the uniform vorticity limit

In this section, we study the linear, temporal stability of the inviscid model in the uniform vorticity limit, i.e. the velocity $u(y)$ is piecewise-linear such that $\omega_+ \to 1$ and $\omega_- \to \beta$ in (2). A solution for the stream function (2) is

$$\begin{aligned}
\psi^{\mathrm{I}} &= \varepsilon A\mathrm{e}^{-k(y-1)}\phi,\\
\psi^{\mathrm{II}} &= -\frac{1}{2}y^2 + y + \varepsilon\left(B\mathrm{e}^{ky} + C\mathrm{e}^{-ky}\right)\phi,\\
\psi^{\mathrm{III}} &= -\frac{\beta}{2}y^2 + \beta y + \varepsilon\left(E\mathrm{e}^{ky} + F\mathrm{e}^{-ky}\right)\phi,\\
\psi^{\mathrm{IV}} &= \varepsilon G\mathrm{e}^{k(y-\frac{1}{\beta})}\phi,
\end{aligned} \tag{6}$$

where the parameter, ε denotes small-amplitude perturbations such that $0 < \varepsilon \ll 1$ and $\phi = \mathrm{e}^{i(kx-\sigma t)}$ denotes traveling waves with frequency, σ, and wavenumber, k. Note that the stream function in both regions I and IV decays to zero as $|y| \to \infty$.

We assume small amplitude traveling wave disturbances to the three interfaces (H_+, H_0, H_-) which demarcate the discontinuities in vorticity between the regions I–IV,

$$H_+ = 1 + \varepsilon\eta_+(x,t),$$
$$H_0 = \varepsilon\eta_0(x,t), \tag{7}$$
$$H_- = \frac{1}{\beta} + \varepsilon\eta_-(x,t),$$

where

$$\{\eta_+(x,t), \eta_0(x,t), \eta_-(x,t)\} = \int_{-\infty}^{\infty} \{\hat{\eta}_+(k), \hat{\eta}_0(k), \hat{\eta}_-(k)\}\phi \,\mathrm{d}k. \tag{8}$$

In order to relate the solutions of the four regions and solve for the coefficients in (6), we apply the interface conditions (5). Solving for the coefficients in equation (6), we obtain the dispersion relation

$$\begin{aligned}(\sigma-k)\left[1+\frac{\beta}{2\sigma}\left(\gamma_-^2+1\right)\right]\left[1+\frac{1}{2\sigma}\left(\gamma_+^2-1\right)\right]\\ = -(\sigma-k)\left[1-\frac{\beta}{2\sigma}\left(\gamma_-^2-1\right)\right]\left[1-\frac{1}{2\sigma}\left(\gamma_+^2+1\right)\right]-(1-\beta)\left[1+\frac{1}{2\sigma}\left(\gamma_+^2-1\right)\right]\left[1-\frac{\beta}{2\sigma}\left(\gamma_-^2-1\right)\right],\end{aligned} \tag{9}$$

where $\gamma_+ = \mathrm{e}^{-k}$ and $\gamma_- = \mathrm{e}^{k/\beta}$. Note that (9) is invariant to the transformation $\hat{\beta} = 1/\beta$, $\hat{\sigma} = -\hat{\beta}\sigma$, $\hat{k} = -k\hat{\beta}$. Based on this transformation, finding the critical wavenumber, k_{cr}, for $-1 \leqslant \beta < 0$ is equivalent to finding the critical wavenumber for $\hat{\beta} \leqslant -1$. The unsteady disturbances described by the dispersion relation are vorticity preserving, and as a result, the total velocity is continuous across the interface. Another solution to the linear system that is allowed by the continuity of pressure boundary condition exists in which the disturbance velocity across the interface is discontinuous. In this case, $A = G = \sigma = 0$ in (6). This convected disturbance results in a discontinuity in the velocity tangent to the interface, i.e. a vortex sheet, that is equal to the strength of the vorticity in the region times the amplitude of the disturbance to the interface, η. Although $\sigma = 0$ for this disturbance, $k \to 0$ as well and the phase velocity is finite. It can be shown that this disturbance convects with the mean velocity at the interface.

The growth rate of the small-amplitude disturbances, σ_{I}, is plotted in Fig. 4(a) as a function of wavenumber, k, for a symmetric shear layer, $\beta = -1$, where σ_{I} is the imaginary part of σ. This corresponds to the case considered by Rayleigh [10]. When $\sigma_{\mathrm{I}} > 0$ the mode is unstable. Three modes are evident. The two nonsymmetric modes are unstable to long wavelength disturbances and are represented by the dotted and long-dashed curves. The modes become neutrally stable above the critical wavenumber, $k_{\mathrm{cr}} \approx 1.84$ in agreement with Rayleigh [10]. This result indicates that nonsymmetric disturbances with critical wavelengths greater than about $1.7D$ should be unstable. Fig. 2 shows a sinuous disturbance with a wavelength of about $3D$, consistent with this result. The solid line in Fig. 4(a) at $\sigma_{\mathrm{I}} = 0$ corresponds to the symmetric (varicose) mode which is neutrally stable for all wavenumbers. This is the mode that exists for the wall-bounded case [10,12–16]. The real part of σ, σ_{R}, for symmetric modes is plotted in Fig. 4(b). The dependence of σ_{R} on wavenumber indicates that the symmetric modes propagate as dispersive waves. However, this does not imply that only unstable nonsymmetric disturbances can be seen in jets. If one assumes the existence of a potential core which lies between the positive and negative vorticity regions, then symmetric disturbances are also unstable to long wavelength disturbances [10]. This implies that as one goes downstream where the potential core has mixed out, nonsymmetric disturbances should dominate.

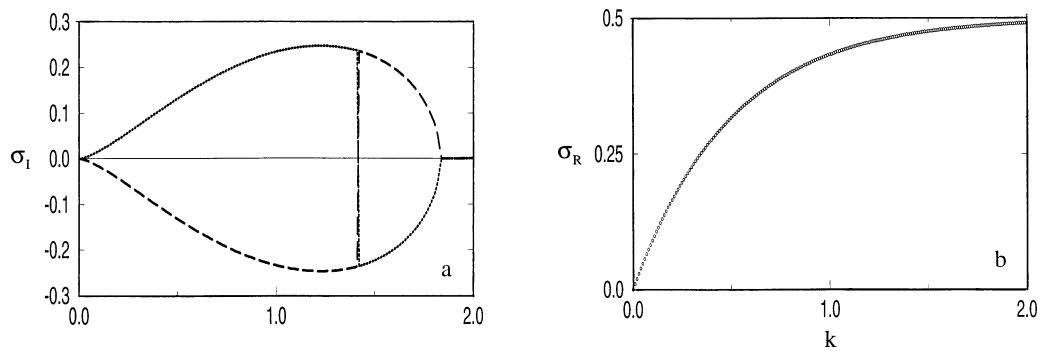

Fig. 4. (a) The growth rate of three modes is plotted as a function of wavenumber for $\beta = -1$. Nonsymmetric modes: dotted (. . . . . .) and long dash (— — —) curves. Symmetric mode: solid curve (———) at $\sigma_{\mathrm{I}} = 0$. When $\sigma_{\mathrm{I}} > 0$, the mode is unstable. (b) The real part of the angular frequency for the neutrally stable mode indicates that it propagates as a dispersive wave.

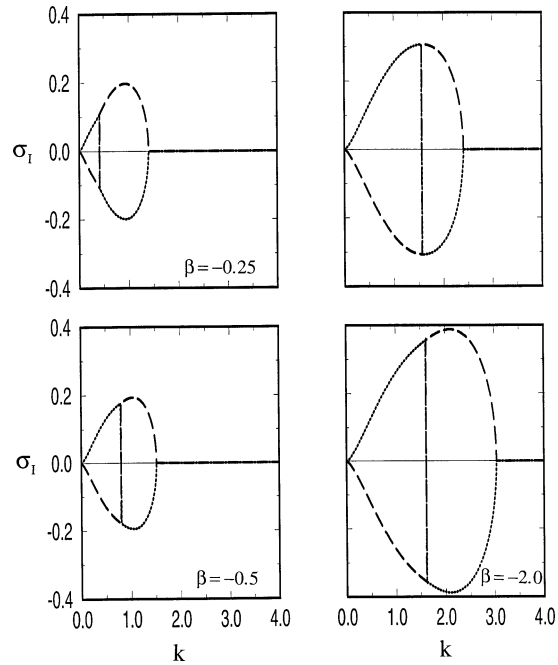

Fig. 5. The growth rate for all three modes is plotted as a function of wavenumber for various degrees of jet asymmetry, β. Nonsymmetric modes: dotted (.....) and long dash (— — —) curves. Symmetric mode: solid curve (———) at $\sigma_I = 0$. When $\sigma_I > 0$, the mode is unstable.

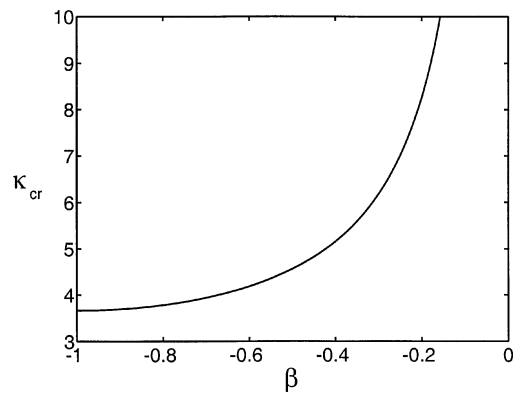

Fig. 6. Dependence of the critical wavenumber on the jet asymmetry, β, showing that the stability decreases with greater asymmetry.

The effect of asymmetry in the jet velocity profile for four cases where $\beta = -0.25, -0.5, -1.5, -2.0$ is shown in Fig. 5. In these cases we observe that varying the relative strength of the positive vorticity to that of the negative vorticity does not result in a qualitative change in the stability of the jet. Small-amplitude waves remain unstable to long wavelength disturbances for the two nonsymmetric modes. These results suggest that finite-amplitude long wavelength disturbances will form sufficiently downstream from the jet exit as the small-amplitude disturbances grow. Note that for the cases $\beta = -0.5$ and $\beta = -2$, $k_{cr} = 1.52$ and $k_{cr} = 3.04$, respectively. This is consistent with the scaling invariance in (9). Physically, $\beta = -0.5$ implies that layer II is half as thick as layer III, whereas for $\beta = -2.0$, layer III is half as thick as layer II. When $\beta = -0.5$, the critical wavelength for instability is a particular dimensional wavelength, λ_{cr}. When $\beta = -2.0$, the critical wavelength for instability is the same dimensional wavelength, λ_{cr}, by symmetry with the $\beta = -0.5$ case. However, since we non-dimensionalize with respect to the upper layer thickness, the nondimensional critical wavelength for $\beta = -2.0$ is half that for $\beta = -0.5$. Likewise, the maximum amplification rate for $\beta = -2.0$ is twice that for $\beta = -0.5$ due to the scaling.

From Fig. 5, it is evident that the stability of the jet is modified by the jet's asymmetry. The dependence of the critical wavenumber on the jet asymmetry is shown in Fig. 6. Here, we scale the critical wavenumber with the total jet width $(H_+^\infty - H_-^\infty)$ rather than with H_+^∞, such that $\kappa_{cr} = k_{cr}(1 - 1/\beta)$, to permit comparison of the critical wavenumber for jets of

identical width but different degrees of asymmetry. The critical wavenumber κ_{cr} increases monotonically from a symmetric jet at $\beta = -1$ to an increasingly asymmetric jet as $|\beta|$ gets smaller, indicating that a larger range of wavenumbers are unstable for more asymmetric jet velocity profiles. The maximum value of the amplification rate, σ_I, changes only a small amount over the range of β shown in Fig. 6, decreasing from a maximum of 0.247 at $\beta = -1.0$ to 0.194 at $\beta = -0.47$.

3.2. Long wave theory: general results

The dispersion relation shows that small amplitude waves are unstable to long wavelength disturbances. As a result, further downstream from the exit, these disturbances will grow and become large in amplitude. We consider the evolution of finite-amplitude, long wavelength disturbances to a shear layer. In this approximation $|\partial H_{(+,0,-)}/\partial x| \ll |\partial H_{(+,0,-)}/\partial y|$ and we introduce the small parameter, ε, so that $|\partial H_{(+,0,-)}/\partial x| = \mathrm{O}(\varepsilon)$. From the kinematic condition at each interface this implies that $\frac{1}{u}\partial H_{(+,0,-)}/\partial t = \mathrm{O}(\varepsilon)$.

This suggests we expand the complex velocity field in powers of ε:

$$(u - iv) = (u - iv)_0 + \varepsilon(u - iv)_1 + \cdots, \tag{10}$$

and introduce the slow variables $T = \varepsilon t$, $X = \varepsilon x$. In the long wave limit, the continuity equation and the kinematic condition (4) become

$$\frac{\partial u_0}{\partial X} + \frac{\partial v_1}{\partial y} = 0 \tag{11}$$

and

$$v_1 = \frac{\partial H_{(+,0,-)}}{\partial T} + u_0 \frac{\partial H_{(+,0,-)}}{\partial X}, \quad y = H_{(+,0,-)}. \tag{12}$$

Solving for the transverse velocity in (11) we obtain

$$v_1(y, X, T) = v_{H_0} - \frac{\partial}{\partial X} \int_{H_0}^{y} u_0 \, \mathrm{d}y - u_{H_0} \frac{\partial u_{H_0}}{\partial X}, \tag{13}$$

where u_{H_0}, v_{H_0} are the leading order streamwise and transverse velocities along the centerline interface, $y = H_0(X, T)$. The vorticity in the shear layer is described by (3), which is rewritten in terms of the slow variables as

$$\frac{\partial \omega}{\partial T} + u_0 \frac{\partial \omega}{\partial X} + v_1 \frac{\partial \omega}{\partial y} = 0, \quad H_- < y < H_+, \tag{14}$$

where $v_0 = 0$ from the continuity equation. Recall that $\omega > 0$ for $H_0 < y < H_+$, and $\omega < 0$ for $H_- < y < H_0$.

Since the flow is irrotational in regions I and IV and the velocity field continuous at the interfaces, we may use Cauchy's formula to express the velocity in terms of its expression along the interfaces H_+ and H_-,

$$(u - iv)^{\mathrm{I,IV}} = \frac{1}{2\pi i} \int_{(H_+, H_-)} \frac{(u - iv)^{\mathrm{II,III}}}{z' - z} \, \mathrm{d}z', \tag{15}$$

where $z = x + iy \in \mathrm{I, IV}$ and $z' \in H_+, H_-$. Evaluating the velocity on the interface (H_+, H_-) using Plemejl's formula we obtain:

$$\begin{aligned} \lim_{y \to H_+} (u - iv)^{\mathrm{I}} &= \left[\frac{1}{2}(u - iv)^{\mathrm{II}} + \frac{1}{2\pi i} \oint_{-\infty}^{\infty} \frac{(u - iv)^{\mathrm{II}}}{X' - X} \, \mathrm{d}X' \right]\Bigg|_{y = H_+}, \\ \lim_{y \to H_-} (u - iv)^{\mathrm{IV}} &= \left[\frac{1}{2}(u - iv)^{\mathrm{III}} - \frac{1}{2\pi i} \oint_{-\infty}^{\infty} \frac{(u - iv)^{\mathrm{III}}}{X' - X} \, \mathrm{d}X' \right]\Bigg|_{y = H_-}. \end{aligned} \tag{16}$$

At the interfaces the velocity is continuous, so $v_0^{\mathrm{I}} = v_0^{\mathrm{II}} = 0$ and $v_0^{\mathrm{IV}} = v_0^{\mathrm{III}} = 0$. Using this result in (16) implies $u_0^{\mathrm{II}} = 0$ and $u_0^{\mathrm{III}} = 0$.

Substituting these results into (12) yields:

$$v_{H_\pm} = \frac{\partial H_\pm}{\partial T} \tag{17}$$

and

$$v_{H_0} = \frac{\partial H_0}{\partial T} + u_{H_0}\frac{\partial H_0}{\partial X}. \tag{18}$$

Substituting (18) into (13) the transverse velocity can be expressed:

$$v_1(X, y, T) = \frac{\partial H_0}{\partial T} - \frac{\partial}{\partial X}\int_{H_0}^{y} u_0 \,\mathrm{d}y. \tag{19}$$

We can thus express the evolution of the upper and lower shear layers by

$$\frac{\partial}{\partial T}(H_\pm - H_0) + \frac{\partial}{\partial X}\int_{H_0}^{H_\pm} u_0 \,\mathrm{d}y = 0. \tag{20}$$

This equation describes the evolution of each jet shear layer for an arbitrary velocity profile. Before considering some specific cases where the jet is subject to either varicose and sinuous disturbances, we utilize the vorticity and momentum equations to derive other properties of the long wavelength disturbances in a jet flow.

Since $\omega = -\partial u_0/\partial y$, the vorticity equation, (14), can be written as

$$\frac{D}{DT}\left(\frac{\partial u_0}{\partial y}\right) = \frac{\partial}{\partial y}\left(\frac{Du_0}{DT}\right) - \frac{\partial u_0}{\partial y}\left(\frac{\partial u_0}{\partial X} + \frac{\partial v_1}{\partial y}\right) = 0.$$

The second term is zero by the continuity equation yielding

$$\frac{\partial}{\partial y}\left(\frac{Du_0}{DT}\right) = 0$$

or

$$\frac{\partial^2 p}{\partial X \partial y} = 0. \tag{21}$$

As a result,

$$p = f(X, T) + g(y, T). \tag{22}$$

The y-component of the momentum equation implies that the pressure is independent of y,

$$\varepsilon^2 \frac{D}{DT} v_1 = -\frac{1}{\rho}\frac{\partial p}{\partial y} = \mathrm{O}\big(\varepsilon^2\big), \tag{23}$$

i.e., $p = f(X, T)$. The x-component of the momentum equation yields:

$$\frac{Du_0}{DT} = -\frac{1}{\rho}\frac{\partial p}{\partial X} = -\frac{1}{\rho}\frac{\partial f}{\partial X}. \tag{24}$$

However, since $u_0 = 0$ at the interfaces, $y = H_\pm$, the x-momentum equation shows there is no acceleration of the fluid particles and the leading order longwave solutions are kinematic, i.e. $\partial p/\partial X = 0$. Thus,

$$\frac{Du_0}{DT} = 0, \tag{25}$$

for any y. If the vorticity is continuous across the interface $y = H_0$, then $\partial u_{H_0}/\partial y = 0$ and the streamwise velocity at the jet centerline is governed by

$$\frac{\partial u_{H_0}}{\partial T} + u_{H_0}\frac{\partial u_{H_0}}{\partial X} = 0, \tag{26}$$

with solutions

$$u_{H_0} = u_0^{\mathrm{I}}\big(\xi, H_0^{\mathrm{I}}(\xi)\big) \tag{27}$$

and

$$X = \xi + u_0^{\mathrm{I}}\big(\xi, H_0^{\mathrm{I}}\big)T, \tag{28}$$

where $H_0^{\mathrm{I}}(\xi) = H_0(\xi, T=0)$ is the deformation of the jet centerline at $T=0$. This solution shows that the streamwise velocity is constant along characteristics moving with the local velocity $u(H_0)$.

Note that by integrating over each shear layer $y \in (H_0, H_+)$, $y \in (H_-, H_0)$ and using the result that $u_0 = 0$ at $y = H_\pm$, Eq. (26) can be expressed, to leading order, as

$$\frac{\partial \Gamma_+}{\partial T} + \Gamma_+ \frac{\partial \Gamma_+}{\partial X} = 0, \qquad \frac{\partial \Gamma_-}{\partial T} + \Gamma_- \frac{\partial \Gamma_-}{\partial X} = 0, \tag{29}$$

where $\Gamma_+ = \int_{H_0}^{H_+} \omega \,\mathrm{d}y$ and $\Gamma_- = \int_{H_-}^{H_0} \omega \,\mathrm{d}y$ are the circulations per unit span or the velocity jumps across each shear layer. The solution to (29) is of the form,

$$\Gamma_\pm = f_\pm[X - \Gamma_\pm T], \tag{30}$$

where $\Gamma_\pm(X,0) = f_\pm(X)$. Eq. (29) indicates that regions of circulation convect downstream with a speed proportional to the local velocity. As a result, regions of higher circulation convect downstream faster resulting in increasing vorticity gradients. This process results in a concentration of regions of vorticity into sharp fronts. Moreover, this result shows that the process of vorticity concentration into sharp fronts is related to the strength and thickness of the shear layer. As a result, the concentrated regions of vorticity which drive the flapping frequency of the jet would be expected to scale with the local vorticity. The velocity jump is equal across each side of the jet, i.e. $\Gamma_+ = \Gamma_-$ suggesting that both sides of the jet will steepen at the same rate.

In the transition region of the jet where the shear layers on opposite sides of the jet have merged, the shear layer thickness is the jet half width. Experiments have shown that when the flapping frequency is non-dimensionalized by local mean-velocity scale and lengthscale the flapping frequency is equal to a constant [5].

The solutions in (30) form shocks, or 'break', at times [17]

$$T_s = \min[-1/f'], \tag{31}$$

where the prime denotes differentiation with respect to X. As an example, we consider an initially slowly varying Gaussian circulation distribution, $\Gamma(X,T)$, characterized by

$$f(X) = 1 + A\mathrm{e}^{-(\frac{X}{\alpha})^2}, \tag{32}$$

where A is the amplitude of the disturbance and α is a parameter related to the wavelength of the perturbation. Then

$$\frac{\mathrm{d}f}{\mathrm{d}X} = \frac{-2AX}{\alpha^2}\mathrm{e}^{-(\frac{X}{\alpha})^2} \tag{33}$$

and breaking takes place at

$$T_s = \frac{\alpha}{A}\left(\frac{\mathrm{e}}{2}\right)^{1/2}. \tag{34}$$

Eq. (34) shows that the timescale for the formation of sharp fronts scales with the initial spatial distribution of the disturbance, α, and inversely with the strength of the disturbance, A. For example, the circulation, $\Gamma_\pm$, is plotted in Fig. 7 for $A = 0.5$ and $\alpha = 1$, based on numerical calculations. The circulation is shown for three time instants, $T = 0,\ 0.45T_s,\ 0.90T_s$. As the

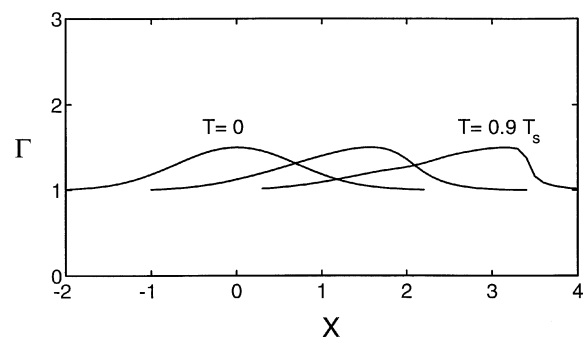

Fig. 7. The steepening of a small amplitude, long wavelength, sinuous Gaussian disturbance $f(X)$ as it propagates in the streamwise direction for $T = 0, 0.45T_s, 0.9T_s$, from left to right.

disturbance propagates downstream, it steepens indicating the formation of sharp fronts of vorticity. The time that breaking occurs for these parameters is $T_s = 2.33$.

In what follows, we consider several vorticity distributions to show that the vorticity distribution has a strong influence on the evolution of the jet and the type of disturbances, sinuous or varicose, which propagate downstream. For a varicose disturbance, the transverse velocity at each interface is antisymmetric or opposite in sign about the jet centerline and for a sinuous disturbance the transverse velocity is symmetric or the signs of the transverse velocity are the same, about the jet centerline. Physically, this means that disturbances to the upper and lower shear layers will move in the same direction for a sinuous disturbance and in opposite directions for varicose disturbances.

3.3. Long wave theory: evolution equation for the jet shear layers

The results of the previous section show that velocity gradients in each jet shear layer will steepen with time. In this section, we derive equations governing the evolution of the interfaces demarcating vortical flow from irrotational flow for a variety of cases with both sinuous and varicose disturbances to determine the conditions under which flapping motion will occur.

3.3.1. Long wave theory: symmetric modes and the wall-bounded jet

We first consider the case where the vorticity in the lower shear layer is the mirror image of the vorticity in the upper shear layer and the disturbances in each shear layer are symmetric. It then follows from continuity of transverse velocity at $y = H_0$ that $v_{H_0} = 0$, $H_0 = 0$ and this corresponds to the case of a slip wall bounding the shear layer. Owing to the complete symmetry about the centerline, we need only consider the upper shear layer, $0 < y < H_+$. Eq. (20) takes the form

$$\frac{\partial H_+}{\partial T} + \frac{\partial}{\partial X}\int_0^{H_+} u_0 \,\mathrm{d}y = 0. \tag{35}$$

We define

$$c(X, H_+, T) = \int_0^{H_+} \frac{\partial u_0}{\partial H_+}\,\mathrm{d}y. \tag{36}$$

The evolution of the interface can then be written:

$$\frac{\partial H_+}{\partial T} + c(H_+, X, T)\frac{\partial H_+}{\partial X} = 0. \tag{37}$$

This equation has the solution

$$H_+ = H^{\mathrm{I}}(\xi) \tag{38}$$

with $H_+^{\mathrm{I}}(\xi) = H_+(\xi, 0)$, $\mathrm{d}X/\mathrm{d}T = c(X, H_+^{\mathrm{I}}(\xi), T)$ and where $X = \xi$ at $T = 0$. This solution shows that the disturbances to the shear layer will propagate with speeds proportional to the initial disturbance amplitude and thus exhibit steepening with time.

3.3.2. Uniform vorticity limit

Another simple case occurs when the vorticity is uniform in each shear layer [10–16]. Note that here the vorticity is discontinuous across the three interfaces and so $\omega_+ \to 1$ and $\omega_- \to \beta$ in (2) and that motion of the centerline can only occur when $\beta \neq -1$. Note that this vorticity distribution differs from that observed in the flow visualization which showed a significant streamwise variation in the vorticity distribution.

In this case, the streamwise velocity field is piecewise linear,

$$u_0^{\mathrm{II}} = -y + H_+(X, T),$$
$$u_0^{\mathrm{III}} = \beta\big(-y + H_-(X, T)\big)$$

and, from (20), the interface evolution equations in both shear layers become

$$\frac{\partial(H_+ - H_0)}{\partial T} + (H_+ - H_0)\frac{\partial(H_+ - H_0)}{\partial X} = 0 \tag{39}$$

and

$$\frac{\partial(H_- - H_0)}{\partial T} + \beta(H_- - H_0)\frac{\partial(H_- - H_0)}{\partial X} = 0. \tag{40}$$

When $\beta = -1$, $H_0 = 0$ and (39), (40), (37) yield

$$\frac{\partial}{\partial T} H_\pm + H_\pm \frac{\partial}{\partial X} H_\pm = 0. \tag{41}$$

Eqs. (39), (40) govern the evolution of the upper and lower shear layers of the jet in terms of the difference in height between the interfaces $H_\pm$ and H_0. Continuity of streamwise velocity at $y = H_0$ implies that $(H_+ - H_0) = \beta(H_- - H_0)$ and that the circulation in the upper and lower shear layers is equal. The solutions to (39) and (40) are of the form

$$\begin{aligned} F_+ &= f_0[X - F_+ T], \\ F_- &= g_0[X - \beta F_- T], \end{aligned} \tag{42}$$

where $F_+ = H_+ - H_0$, $F_- = H_- - H_0$ and where $F_+(X, 0) = f_0(X)$ and $F_-(X, 0) = g_0(X)$. In the limit of symmetric disturbances for which $\beta = -1$ and $H_0 = 0$, the system reduces to the wall-bounded shear layer result and indicate that in the uniform vorticity case the parameter beta plays an important role since a transverse velocity at the jet centerline can only exist when $\beta \neq -1$. The solutions (42) indicate that the higher portions of the interface will propagate downstream faster than the lower portions resulting in the steepening of the interface and the formation of steep positive and negative vorticity fronts. This result is not unexpected since in the limit of uniform vorticity the magnitude of the circulation per unit span is associated with the height of the interface.

Evaluating (19) at each interface and noting that $(H_+ - H_0) = \beta(H_- - H_0)$, the normal velocity satisfies the condition, $\operatorname{sgn}\{v_1(y = H_+)\} = -\operatorname{sgn}\{v_1(y = H_-)\}$. Thus, for a uniform vorticity distribution only varicose disturbances can occur and we must consider more general jet velocity profiles to obtain the flapping motion observed in the experiments.

3.3.3. Long wave theory: sinuous disturbances and flapping motion

Although the uniform vorticity case offers some insight into the steepening of the jet it does not allow finite amplitude sinuous motions of the jet. Moreover, the flow visualization suggests that the flapping motion of the jet occurs when there is a 'vortex-street' type of alignment of the vortices causing motion of the jet centerline. In this section, we look for solutions to the jet centerline which exhibit flapping. We define the jet centerline to be a material interface along which the vorticity is zero since along this interface the vorticity is transitioning from positive to negative as one crosses the upper shear layer to the lower shear layer.

Since we are looking for solutions to sinuous disturbances, we are interested in solutions where the transverse velocity has the same sign in both shear layers. As a special case, we assume v_1 is a symmetric about $y = H_0$, i.e., $v_1(y - H_0) = v_1(H_0 - y)$ and thus from the y-momentum equation the pressure is also symmetric, i.e.,

$$\frac{\partial v_1}{\partial y} = \frac{\partial p}{\partial y} = 0, \quad y = H_0. \tag{43}$$

By continuity,

$$\frac{\partial u_0}{\partial x} = 0, \quad y = H_0, \tag{44}$$

or u_{H_0} is constant. Using (43), the y-momentum equation takes the final form

$$\frac{\partial v_1}{\partial T} + u_{H_0} \frac{\partial v_1}{\partial X} = 0, \tag{45}$$

and the transverse velocity, v_1, has the solution

$$v_1 = V(X - u_{H_0} T). \tag{46}$$

The evolution of sinuous disturbances at the jet centerline are described by the evolution equation

$$V(X - u_{H_0} T) = \frac{\partial H_0}{\partial T} + u_{H_0} \frac{\partial H_0}{\partial X}. \tag{47}$$

The centerline interface thus has solutions of the form

$$H_0 = F(X - u_{H_0} T) + \frac{X}{u_{H_0}} V(X - u_{H_0} T). \tag{48}$$

This result shows that sinuous disturbances will propagate with a constant velocity equal to the initial centerline velocity. Moreover, the disturbances will grow linearly as they convect downstream. This result also shows that the flapping motion will become more pronounced as one moves downstream which is consistent with experimental observations. In the more general case where the transverse velocity is not a symmetric function about $y = H_0$ an analytic solution for the jet centerline cannot be found. However, it is expected that the disturbances will grow algebraically and also steepen as they propagate downstream.

4. Discussion

The flapping motion in a two-dimensional turbulent jet has been attributed to two causes: (1) a lateral oscillatory motion of the entire flow field resulting from a traveling wave instability, (2) a sequence of coherent structures alternating in sign on either side of the jet [4–7]. The preferred explanation attributes the flapping to organized coherent structures based on comparing the flapping frequency to the frequency of intermittent structures in the turbulent jet. In fact, Oler and Goldschmidt attempted to model the flapping motion as a superposition of a series of Rankine vortices arranged as a vortex street [18]. The problem with attributing the flapping to a series of coherent structures that supposedly drive the flapping motion is that there is no explanation for the origin of the coherent structures themselves.

In the analysis presented in this paper, we do not pre-suppose any organized coherent structures but instead consider the stability of the simplified flow field. The results of the linear inviscid analysis show that in the transition region where the jet core has mixed out long wavelength antisymmetric disturbances are unstable and will grow to finite amplitudes whereas symmetric disturbances are neutrally stable. The conclusions of the nonlinear finite-amplitude analysis are that (1) through a nonlinear steepening mechanism concentrated regions of vorticity will develop into sharp fronts of vorticity, (2) the formation timescale of these regions scales with the local vorticity, (3) the concentrated regions of vorticity convect downstream with the local mean velocity, (4) the flapping motion results for sinuous disturbances which occur only for nonuniform vorticity distributions and (5) the flapping motion grows linearly with downstream distance. These conclusions are in agreement with experiments which attribute the flapping of the jet to a traveling wave instability (sinuous) which leads to a sequence of coherent structures alternating in sign (asymmetric) on either side of the jet and whose strength scales with the local vorticity [4–7].

The simple experiment visualizing the flow in the transition region of a planar jet shown in Fig. 2 links the proposed causes for flapping (traveling wave instability and coherent structures) to the results of our analysis. The initial slow variation in the streamwise direction and oscillation of the overall jet field is related to the sinuous (nonsymmetric) structure of the instability. The motion is sinuous near the jet exit but it leads to coherent circular motions further downstream that eventually drive the finite-amplitude centerline motion which grows and steepens as it convects downstream. Our analysis describes the development of vorticity fronts which convect downstream with the local mean flow and the motion of the jet centerline resulting from finite-amplitude sinuous disturbances. Strong streamwise variation in circulation is evident in Fig. 2 where the circulation changes from positive to negative and back to positive over a small streamwise distance. A schematic of the vortex-jet system, which drives the flapping motion corresponding to the flow visualization, is shown in Fig. 8. The vortex-jet consists of three vortices and a streakline in the jet core indicated by the dark curve. At point A, vortices 1 and 2 dominate the local flow pushing the jet up. At point B, vortex 2 dominates the local flow driving the jet down and at point C vortex 3 dominates the local flow pushing the jet up again. The resulting vortex-system continues the flapping motion of the jet further downstream of the initial sinuous disturbance. This motion plays an important role in the entrainment of irrotational fluid into the planar jet and the mixing of the jet with the ambient fluid.

The results of this paper suggest that attempts to control the mixing properties of the jet should focus on (1) attempts to modify the shear layer or (2) attempts to excite symmetric modes to prevent or modify the vortex system which drives the flapping motion. Further experiments are necessary to show more time sequences, the velocity field over a greater streamwise extent, and the evolution of the jet vorticity to validate the analytical results presented in this paper.

Finally, a special case of the model presented here occurs when one considers only symmetric disturbances in a uniform layer of vorticity. This case satisfies impermeability at the line of symmetry and thus may model a wall-bounded shear layer. In particular, Jimenez and Orlandi studying the formation of vortices in a turbulent channel showed that a vortex layer in the neighborhood of a slip wall tends to roll into discrete vortices via nonlinear steepening [12]. Furthermore, they conjectured that dispersive effects may act to explain the persistence of these discrete vortices. The current work generalizes the work of Jimenez and Orlandi to unbounded flows such as jets and examines the effect of vorticity distribution on the motion of the jet. By analogy to the wall-bounded work, we conjecture that dispersive effects may act in the jet model and explain the persistence of the antisymmetric structures.

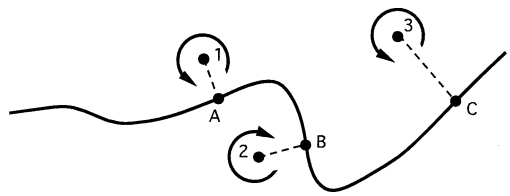

Fig. 8. Schematic of the vortex-jet system corresponding to the visualization in Fig. 2.

Acknowledgement

We acknowledge helpful discussions with Lars Pantzlaff and Steve Wereley on the experimental set-up and the assistance of Alp Akonur in the preparation of this paper.

References

[1] L.J.S. Bradbury, The structure of a self-preserving turbulent plane jet, J. Fluid Mech. 23 (1965) 31–64.
[2] V.W. Goldschmidt, P. Bradshaw, Flapping of a plane jet, Phys. Fluids 16 (1973) 354–355.
[3] W. Everitt, A.G. Robins, The development and structure of turbulent plane jets, J. Fluid Mech. 88 (1978) 563–583.
[4] J.W. Oler, V.W. Goldschmidt, Interface crossing frequency as a self-preserving flow variable in a turubulent plane jet, Phys. Fluids 23 (1980) 19–21.
[5] J.C. de Gortari, V.W. Goldschmidt, The apparent flapping motion of a turbulent plane jet – further experimental results, J. Fluids Eng. 103 (1981) 119–126.
[6] J.C. Mumford, The structure of the large eddies in fully developed turbulent shear flows. Part 1. The plane jet, J. Fluid Mech. 118 (1982) 241–268.
[7] R.A. Antonia, L.W.B. Browne, S. Rajagopalan, A.J. Chambers, On the organized motion of a turbulent plane jet, J. Fluid Mech. 134 (1983) 49–66.
[8] R.A. Antonia, A.J. Chambers, D. Britz, L.W.B. Browne, Organized structures in a turbulent jet: topology and contribution to momentum and heat transport, J. Fluid Mech. 172 (1986) 211–229.
[9] H. Li, T. Nozaki, Application of wavelet cross-correlation analysis to a plane turbulent jet, JSME Inter. J., Series B 40 (1997) 58–66.
[10] J.W.S. Rayleigh, The Theory of Sound, Vol. II, 2nd ed., Macmillan, London, 1896, pp. 394–396.
[11] M.E. Stern, S.I. Voropayev, Formation of vorticity fronts in shear flow, Phys. Fluids 27 (1984) 848–855.
[12] D.I. Pullin, P.A. Jacobs, R.H.J. Grimshaw, P.G. Saffman, Instability and filamentation of finite-amplitude waves on vortex layers of finite thickness, J. Fluid Mech. 209 (1989) 359–384.
[13] O. Atassi, Analytical and numerical study of the nonlinear interaction between a point vortex and a wall-bounded shear layer, J. Fluid Mech. 373 (1998) 155–192.
[14] D.I. Pullin, The nonlinear behaviour of a constant vorticity layer at a wall, J. Fluid Mech. 108 (1981) 401–421.
[15] M.E. Stern, L.J. Pratt, Dynamics of vorticity fronts, J. Fluid Mech. 161 (1985) 513–532.
[16] J. Jiménez, P. Orlandi, The rollup of a vortex layer near a wall, J. Fluid Mech. 248 (1993) 297–313.
[17] G.B. Whitham, Linear and Nonlinear Waves, Wiley, New York, 1974, pp. 22–23.
[18] J.W. Oler, V.W. Goldschmidt, A vortex-street model of the flow in the similarity region of a two-dimensional free turbulent jet, J. Fluid Mech. 123 (1982) 523–535.